

Bio-impedance identification of fingertip skin for enhancement of electro-tactile-based preference

John Gregory¹ · Shengchun Tang^{2,3} · Yudong Luo⁴ · Yantao Shen⁴

Received: 16 August 2016 / Accepted: 15 December 2016 / Published online: 16 January 2017
© Springer Singapore 2017

Abstract Research in rehabilitation engineering has shown that electrodes can produce tactile sensations with appropriate electrical signals to stimulate the multiple tactile receptors located under the fingertip skin. Numerous equivalent skin–electrode interfaces have been modeled to characterize the electrical properties of the skin; however, the values of these circuit models are continually changing, due both to the nonlinearity associated with human fingertip skin and to individual user differences. As a result, electrical stimulation that is suitable in terms of current or voltage level for tactile sensations cannot be guaranteed for every user. An identification method is then necessary for characterizing the parameters of the skin–electrode interface circuit model so as to improve rendering consistency and comfort for every user regardless of skin condition. In this paper, we introduce a custom-built electro-tactile display terminal, and then using this display terminal for data collection, we present an online identification scheme for

determining the bio-impedance parameters of the well-known Cole–Cole circuit model for the skin–electrode interface. For this, a modified Kalman least squares iterative approach is used that relies on measuring only one-port square wave stimulation voltages. The repeatability and reliability of the identification scheme are tested by identifying the resistor–capacitor (RC) load bio-impedance networks of different users with both a dry and slightly damp index fingertip over multiple identification trials. Additionally, because of the inevitable variation in the parameters over multiple measurements, the repeatability of multiple calculated RC models (dry and wet) is further evaluated. The significance of our work is that it greatly improves the tactile rendering performance of electrical stimulation (electro-tactile) systems and will benefit the development of electro-tactile-based rehabilitative robotic devices and human–robot interfaces.

Keywords Electro-tactile rendering display · Electrode array · Haptic devices · Rehabilitative robot devices · Fingertip · Skin–electrode interface · Bio-impedance · Identification

✉ Yantao Shen
ytshen@unr.edu

John Gregory
gregor87@gmail.com

Shengchun Tang
tangshengchun@bistu.edu.cn

Yudong Luo
yluo@unr.edu

¹ Coritech Services and TM3 Systems, Michigan, USA

² School of Automation, University of Science and Technology Beijing, Beijing 100083, China

³ School of Electrical Engineering, Beijing Information Science and Technology University, Beijing 100192, China

⁴ Department of Electrical and Biomedical Engineering, University of Nevada, Reno, NV 89557, USA

1 Introduction

The placement of electrodes designed to substitute touch sensation has been performed in various locations on the body for sensory rehabilitation. For example, the tongue (Kaczmarek and Tyler 2000; Bach-y-Rita et al. 1998a, b), the abdomen (Haase and Kaczmarek 2005), and fingertip (Koo et al. 2006; Kaczmarek et al. 1994; Shimojo et al. 2003; Szeto and Riso 1990; Szeto and Saunders 1982; Bobich et al. 2007; Kajimoto et al. 2002, 2004) are the areas most commonly studied to assess the ability of

human subjects to detect and identify patterns using these devices. This research has shown that electrical stimuli can effectively deliver a significant amount of information about patterns of stimuli; thus, ample research supports the notion that electrical stimuli are a viable means for delivering sensory information in rehabilitation therapy (Kaczmarek and Webster 1991).

Our research interest pertains to the ability to induce touch sensations on the fingertip skin using an electrode array; this mechanism, also called electro-tactile stimulation or electro-cutaneous stimulation, is illustrated in Fig. 1. The fingertip skin consists of several horizontal layers. Seven classes of mechanoreceptors, two classes of thermoreceptors, four classes of nociceptors, and three classes of proprioceptors are found within these layers of the skin. To an extent, they provide the perceived tactile sensations during mechanical or electrical stimulation (Kajimoto et al. 2002, 2004; Poletto and Doren 1999; Kaczmarek and Webster 1991; Asamura et al. 1999; Vallbo and Johansson 1984; Kajimoto et al. 1999). Different receptors sense different tactile modalities, such as pressure, texture vibration, temperature, and electric voltage or current. Among the various classes of mechanoreceptors, the most commonly investigated tactile receptors include Merkel cells for pressure sensation, Meissner's corpuscle for low-frequency vibration, and deep Pacinian corpuscle for high-frequency vibration (Kajimoto et al. 2004; Kaczmarek and Webster 1991; Vallbo and Johansson 1984), as illustrated in Fig. 2 (adapted from Kajimoto et al. 2004). Several research findings in the areas of psychophysics, neurocytology, electrochemistry, and cognitive science have shown that mechanical or electrical stimulation to these mechanoreceptors produces tactile feelings in humans (Bobich et al. 2007; Faes and Meij 1999; Pliquet et al. 1995; Foster and Lukaski 1996; Phillips and Johnson 1985; Neuman 1998; Reilly 1992; Vallbo 1981; Rattay 1990). Following on these explorations, extensive research in rehabilitation engineering has been performed to elucidate the properties, characteristics, and mechanisms underlying the sensation of touch delivered through electrode arrays on the fingertip skin (Koo et al. 2006; Kaczmarek et al. 1994; Shimojo et al. 2003; Szeto and Riso 1990; Szeto and Saunders 1982;

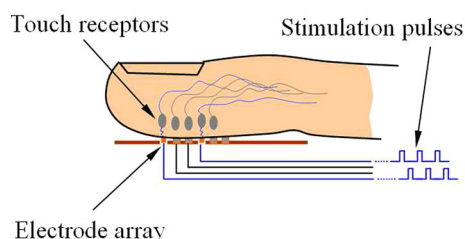


Fig. 1 Illustration of fingertip electro-tactile stimulation through electrode arrays

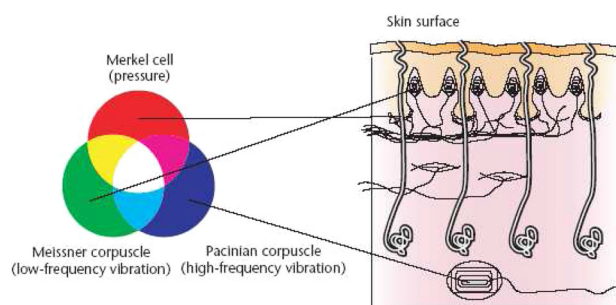


Fig. 2 The mechanoreceptors in human skin. Adapted from Kajimoto et al. (2004)

Bobich et al. 2007; Kajimoto et al. 2002, 2004; Yoon and Yu 2008). Such electro-tactile research and development has provided the potential for advancement of assistive, diagnostic, and rehabilitative devices such as Braille readers, sensory substitution, teleoperation and telepresence, and computer games (Koo et al. 2006; Shimojo et al. 2003; Shen 2007; Shen et al. 2006; Pliquet et al. 1995; Benali-Khoudja et al. 2004; Gemperle et al. 2001; Rossi 2005; Yarimaga et al. 2005a, b; Kajimoto et al. 1999).

However, despite the considerable progress in electro-tactile display technology, such electro-tactile stimulation can be uncomfortable because of the highly variable conditions at the electrode–skin interface (Kaczmarek and Webster 1989). Associated with the sensation quality, the stimulation voltage/current level through the electrodes to the skin must be carefully and accurately controlled according to the user's tactile preference so as to avoid unpleasant sensations. Since the desired current is highly dependent on the electrical impedance parameters of the skin–electrode interface such as skin resistance and capacitance, the sensation will vary with electrode properties and the skin conditions of different users. These impedance parameters must be carefully identified and calibrated before electrical stimulation. In this paper, we focus on developing an identification method to extract those bio-impedance parameters for electro-tactile enhancement. The goal of our work is to identify the parameters online and to use them to automatically tune the voltage/current to a desired sensation level for each user. We believe that our work will provide an effective user-friendly solution to electro-tactile technology.

To reach our research goal, we first developed an electro-tactile display terminal for the index fingertip. By employing this electrical stimulation terminal, and selecting the well-known Cole–Cole skin–electrode circuit model (Foster and Lukaski 1996), we designed a modified Kalman least squares iterative approach that relies on measuring only one-port square wave voltages for identification of the model parameters. We tested the repeatability and reliability of this identification scheme by

identifying the resistor–capacitor (RC) load impedance networks of both dry and slightly damp index fingertip skin of users over multiple identification trials. In addition, because these parameters will inevitably vary over multiple measurements, we further evaluated the repeatability of multiple calculated RC models (dry and wet). Note that the objective of our identification system is to enhance electro-tactile rendering consistency and comfort for every user regardless of skin condition. The work can certainly benefit the user’s sensory experience and motivate one towards a goal of online identification of both the driver circuit Thévenin port impedance and the RC bio-impedance values of the fingertip and electrode interface. As perception levels and skin electrical properties are identified online, the quality of electro-tactile-based sensation/stimulation can be enhanced. One potential application scenario is that the method could be further improved for use in co-robotic rehabilitation systems that help a home therapist stimulate certain skin areas and/or monitor the progress of possible sensorimotor recovery.

This paper is structured as follows: Skin electrical properties and skin–electrode interface models are reviewed in Sect. 2. Based on the equivalent Cole–Cole skin–electrode circuit model, the proposed bio-impedance identification methods are described in Sect. 3. In Sect. 4, the developed custom-built electro-tactile display system and output waveforms are introduced. Then, by employing this developed system, we conduct extensive experiments to verify the proposed methods. The experimental validation and the identification results are then demonstrated and analyzed. Finally, we conclude the work in Sect. 5.

2 Equivalent skin–electrode circuit models

2.1 Circuit model and parameters

The task of transcutaneous electrical stimulation is to overcome the impedance of the skin to activate the receptor or sensory nerves underlying the surface (Dorgan 1999). The surface electrode–skin problem can be presented by an equivalent circuit of the electrodes and its interface with the skin. Under the surface electrodes, characterizing the skin resistance and capacitance should allow for an accurate equivalent circuit model for human skin. The simplest, yet effective, equivalent circuit model that can be used to represent skin impedance is a parallel network consisting of a capacitor and resistor, followed by a series resistor (Dorgan 1999; Poletto and Doren 1999; Kaczmarek and Webster 1989, 1991). The parallel capacitor and resistor, C_p and R_p , in this model represent the electrical properties

of upper stratum corneum (SC), and the series resistor, R_s , represents the impedance of the subdermal medium. The more complete model would consider the skin as composed of numerous layers of cells, each having capacitance and conductance (Dorgan 1999; Rosell and Colominas 1988; Poletto and Doren 1999; Kaczmarek and Webster 1991; Foster and Lukaski 1996; Boxtel 1977; Kaczmarek and Webster 1989).

2.2 Selected skin–electrode interface model for identification

Our parameter identification of the skin bio-impedance model, based on the well-known Cole–Cole function circuit model, is shown in Fig. 3. For an in-depth discussion of this representation, please see Foster and Lukaski (1996). We assume small stimulation currents as measured in the low- to sub-milliamp regime that suffice for the model. Here, R_p represents extracellular compartments in the stratum corneum (SC) such as pores and pathways through the laminar bilayers (Pliquett et al. 1995); C_p models the hydrophobic lipid membranes and laminar bilayer composition that separate extracellular and intracellular corneocyte components; and R_s represents the intracellular pathways through the corneocytes and underlying bulk tissue resistivity, and dominates as the frequencies become high (see Brannon 2009 for physical structure). As mentioned above, R_p is usually the largest resistive element (20 k Ω to 1 M Ω). The typical ranges of C_p are on the nanofarad to sub-nanofarad order (normalized to our electrode dimensions) (Prokhorov 2000; Poletto and Doren 1999; Kaczmarek and Webster 1991). Also, R_s is low, in the kilo- to sub-kilo-ohm range. We neglected the inverse relationship between R_p and current amplitude, since our stimulation currents are about 0.2 mA (dry skin) to 2.5 mA (wet skin). These currents are typical for electrocutaneous display systems with our electrode area dimension (0.454 mm²). The value of R_p is shown to be relatively

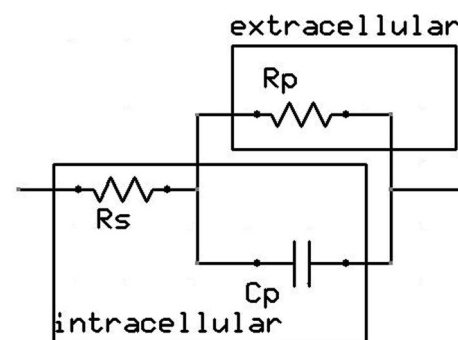


Fig. 3 Cole–Cole-based interface model for small stimulation currents less than about 5 mA

static with respect to our current levels (Dorgan 1999). In general, the sensation threshold versus current amplitude increases with electrode size, along with SC nonlinearity (Dorgan 1999; Kaczmarek and Webster 1991; Pliquett et al. 1995).

3 Identification methodology

The focus of this section is the presentation of a reliable online identification method for calculating the assumed elements of the bio-impedance and the display driver circuit model. Our novel system identification approach calculates both the Z_{th} of the driver circuit of the electro-tactile display and RC-modeled bio-impedance load at the output, as displayed in Fig. 4, by sampling output voltage waveforms in unloaded and loaded states. Note that the unloaded states means there is no fingertip skin engaged or no modeled RC circuit engaged. The loaded state represents the conditions during the engagement of dry or damp fingertip skin or the modeled RC circuit. The Z_{th} is the driver circuit's non-ideal Thévenin impedance and is usually a constant value for the electrode–skin interface. For more details about the driver circuit of the electro-tactile display and the Z_{th} , please see the Appendix and Sect. 4 A. In this paper, our identification method will first be applied to solve/decouple Z_{th} offline from the electrode–skin interface, and then to identify the left RC-modeled bio-impedance load from the fingertip or the model's RC circuit. To start the identification, it is assumed that the original input for the driver's transformers are square wave pulses with programmed amplitudes, pulse frequencies, and duty cycles presented in Table 1. Using this approach, we create one-port measurements that reduce parameter estimation complexity, since the Thévenin voltage need not be identified, as discussed below.

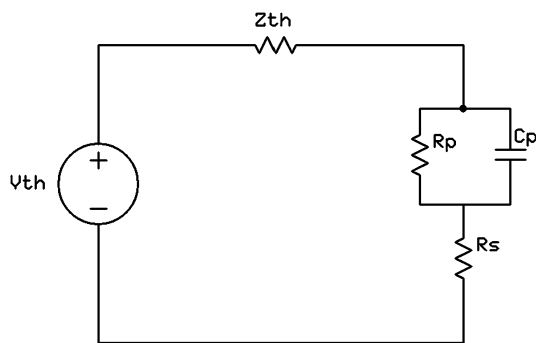


Fig. 4 V_{th} is the measured unloaded output. Z_{th} represents the fifth-order equivalent impedance of the step-up transformer of the display driver. The output under RC load is the first-order bio-impedance model

Table 1 Unloaded square wave stimulation waveform characterization

Output amplitude	Input amplitude	Frequency	Duty cycle
50 V	4.2 V	60 Hz	4%

3.1 Data acquisition for identification

The process starts by sampling the unloaded output of the system at a frequency of 175 kHz using a high-speed data acquisition (DAQ) board (PCI-DAS6025; Measurement Computing Corporation, Norton, MA, USA). The unloaded output is equivalent to the circuit Thévenin output voltage and will be taken as the new sampled input for all future identification. The new sampled output under load consists of known resistor values or human index fingertip skin parameters for either Thévenin or bio-impedance identification, respectively. The sampled input and output undergo separate linear transformations, depending on the desire to identify the circuit or human parameters. To avoid loading the output node from the input side of the DAQ, as well as to linearly scale down the high voltage output to meet the dynamic range constraints of the DAQ, we developed a specialized voltage follower circuit. The circuit scales down the large output voltage amplitude to meet the dynamic range of the DAQ (0.0535 scale factor). Figure 5 shows the schematic of the voltage divider/follower used for DAQ acquisition. As can be seen, we also use a first-order low-pass filter network to filter out system noise. The LM837 operational amplifier (OpAmp) was chosen for its favorable slew rate and signal-to-noise ratio (SNR) characteristics. We also designed it to eliminate bias current error so as not to influence the identification algorithm.

3.2 Identification algorithm

For the identification algorithm, we incorporated and modified the established Kalman successive iteration least-squares method (Steiglitz and McBride 1965). The algorithm first minimizes the output error energy cost function for $i = 0$:

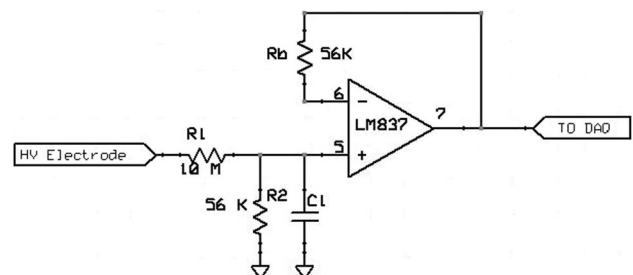


Fig. 5 Schematic of voltage divider/follower designed for DAQ acquisition

$$E = \oint \left| X \frac{N_i}{D_{i-1}} - W \frac{D_i}{D_{i-1}} \right|^2 dz = \oint \left| X \frac{N_i}{D_i} - W \right|^2 \frac{D_i^2}{D_{i-1}^2} \frac{dz}{z}, \tag{1}$$

for $i = 1, 2, 3, \dots$, and $D_0 \leq 1$ of the finite impulse response (FIR)-modified system illustrated in Fig. 6. Note that \mathbf{X} and \mathbf{W} are the respective sampled input and output vectors, and \mathbf{N} and \mathbf{D} represent the unknown one-port rational function numerator and denominator parameter vectors α and β , respectively, of an assumed order that we wish to identify. This system is iterative and pre-filters the input and output with each instance of the previously solved denominator parameter set for $D_0 \leq 1$. The initial global minimum gradient solution to Eq. (1) for $i = 0$ is:

$$\delta = \mathbf{Q}^{-1}\mathbf{c}. \tag{2}$$

where

$$\delta = \begin{pmatrix} \alpha \\ -\beta \end{pmatrix}. \tag{3}$$

\mathbf{Q} and \mathbf{c} are the correlation matrix and parameter vector, respectively. For higher-order systems, large matrix condition numbers of the correlation matrix usually ensue, causing potentially erroneous solutions from bad scaling. For practical solutions, we properly re-scale the correlation matrix using successive singular value decomposition of \mathbf{Q} in Eq. (2). Over many iterations, the minimized output error energy becomes the true error of the infinite impulse response (IIR) error system asymptotically if the denominator quotient in Eq. (1) converges. Realistically, it is not always necessary to implement deep iterations, as the two system errors are similar if the unknown z -domain poles lie close to the origin of the unit circle or quickly converge. Additionally, this least squares algorithm can be implemented recursively for online identification (Ljung 1983).

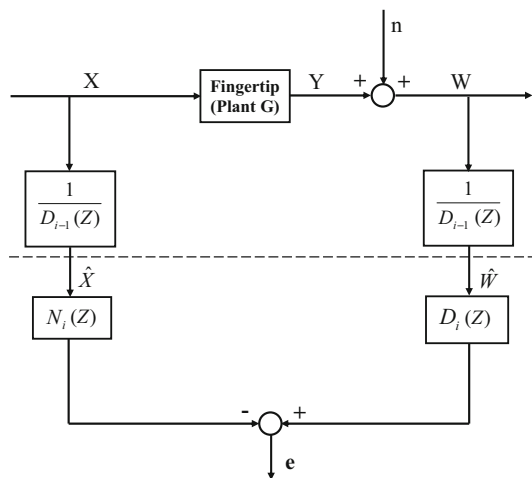


Fig. 6 The iterative pre-filtering scheme for the identification

For each iteration i , we compare the actual output to the calculated output using root relative squared error goodness-of-fit criteria (RRSE):

$$\text{RRSE}_i = \sqrt{\frac{(\mathbf{V}_i - \mathbf{W}) \bullet (\mathbf{V}_i - \mathbf{W})}{(\mathbf{W} - \mathbf{W}_\mu) \bullet (\mathbf{W} - \mathbf{W}_\mu)}}, \tag{4}$$

where \mathbf{V} is the predicted output vector, \mathbf{W} the measured output vector, and \mathbf{W}_μ the mean of the actual output for a given iteration. \bullet represents the scalar product. We chose this metric so that linear signal scaling would not influence the comparison of error magnitudes.

4 Algorithm implementation and evaluation of experimental results

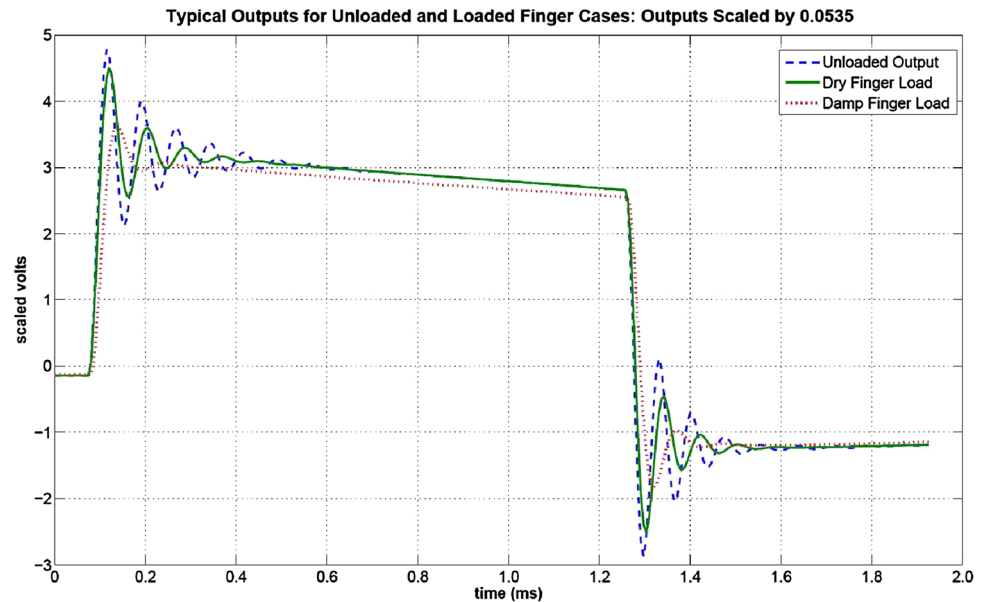
4.1 Display driver output waveforms and Zth

The algorithm implementation relies on a custom-built electro-tactile display including electrode arrays and the display driver circuit (see Appendix). The typical outputs of both the unloaded (no fingertip skin or modeled RC circuit engaged) and loaded (with dry or damp fingertip skin or the modeled RC circuit engaging) terminals of the developed electro-tactile display (see Appendix) are the voltage square waves with duration as shown in Fig. 7.

The main difficulties in, first, achieving and then maintaining signal output quality and integrity include the following: (1) the open-loop system offers no correction for the significant transient response seen at the front and tail of the waveform due to large inductive and capacitive effects; (2) voltage droop observed at steady state occurs due to resistivity in the wires of the incorporated step-up transformers; and (3) bio-impedance load changes between individuals and as a function of the individual’s dermis structure and conditioning may change significantly over time, electrode position, and contact situation. For (1), snubber circuits at the output may be employed to reduce the effect of the transient response. As for (3), similar results have been reported in other works. Rosell et al. showed that impedance decreased 20% at a single stimulation point over a short time, which was attributed to electrolyte penetration through the skin from an applied electric field (Rosell and Colominas 1988). Prokhorov et al. also provided evidence that electric skin impedance changed suddenly and drastically at small millimeter-sized regions of the skin, which they deemed biologically active points (BAPs) (Prokhorov 2000).

In addition, the steady-state level shifts resulted from the driver circuit’s non-ideal Thévenin impedance, Z_{th} . This phenomenon is most pronounced with a damp, chemically

Fig. 7 Typical terminal output waveforms both with fingertip loads and with no load, scaled by 0.0535



treated, or physically altered fingertip, such that the bio-impedance approaches the lower order of magnitude of Z_{th} . The problem then depends on either somehow reducing the skin parameter variations or producing an adequate model of the bio-impedance for closed-loop compensation. The latter approach involves online identification of the physical parameters of the skin so as to tailor the output voltage or current signal based on the user's bio-impedance signature. To identify the bio-impedance signature, we first need to identify/decouple the Z_{th} from the signals offline, as the Z_{th} is a constant value for the electrode–skin interface.

4.2 Offline identification of driver circuit impedance Z_{th}

We tested the described algorithm by identifying the parameters of a fifth-order model of the driver circuit transformers' Thévenin impedance Z_{th} :

$$Z_{th} = \frac{\alpha_0 + \alpha_1 z^{-1} + \dots + \alpha_{n-1} z^{-(n-1)}}{1 + \beta_1 z^{-1} + \dots + \beta_n z^{-n}}, \quad (5)$$

where the parameters α_i and β_i are defined in Eq. (3). The system order is based in part on the non-ideal driver's transformer parasitic effects such as winding leakage inductance, resistance, intra-winding capacitance, and magnetizing inductance [31]. The sampled input is the unloaded Thévenin voltage V_{th} , and the output V_{out} is measured using a known load value of $R_L = 98.8K\Omega$ attached across one of the stimulating electrodes and return path. Using this data, the algorithm solved the impedance parameters based on the derived relation:

$$N_{th_i} V_{out} = D_{th_i} [R_L (V_{th} - V_{out})], \quad (6)$$

where

$$X = V_{out} \quad \text{and} \quad W = [R_L (V_{th} - V_{out})], \quad (7)$$

are the new input and output vectors as depicted in Eq. (1). N_{th_i} and D_{th_i} represent the i th estimation of the Z_{th} one-port numerator and denominator, respectively. Figure 8 compares a trial of the measured and simulated output under the known R_L in Eq. (6) using the identified Z_{th} . The RRSE gives a good result of less than 1% in the comparison. Figure 9 shows the magnitude frequency response of Z_{th} . We noted from the frequency response that the transformer's impedance passed low frequencies (up to 300 Hz) with average impedance of 4.5 $K\Omega$. The impedance steadily increased for higher frequencies, stemming from the large transformer inductive reactance. At about 12 KHz, Z_{th} resonance resulted with 200 $K\Omega$ impedance. This marks the point where the circuit transitions from inductive to capacitive reactance.

To test the prediction accuracy and validity of the previously identified Z_{th} one-port in Eq. (5), and the identification method in general, we simulated the outputs of identified system models and compared them to the measured outputs of known resistive loads via a rearrangement of Eq. (6). Resistor values of $R_{actual} = 21.62, 55.20, 216.6, 328.9, \text{ and } 555.0K\Omega$ were successively attached and the output sampled to fit a Z_L model to each. The values of the resistors realized a proper range of the reported values of human DC skin resistance for various skin moisture content at our electrode dimensions and were selected for this reason (Prokhorov 2000). As our method is reliable and identified Z_{th} over multiple test loads, the assumed

Fig. 8 Identified Z_{th} using a 98.8 k Ω reference load. Output is scaled by 0.0535

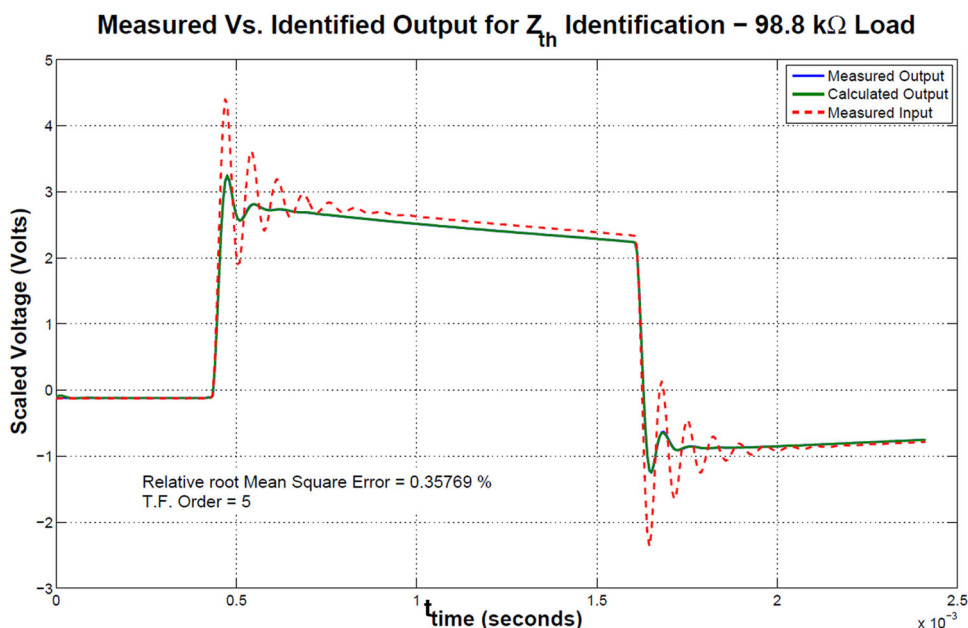
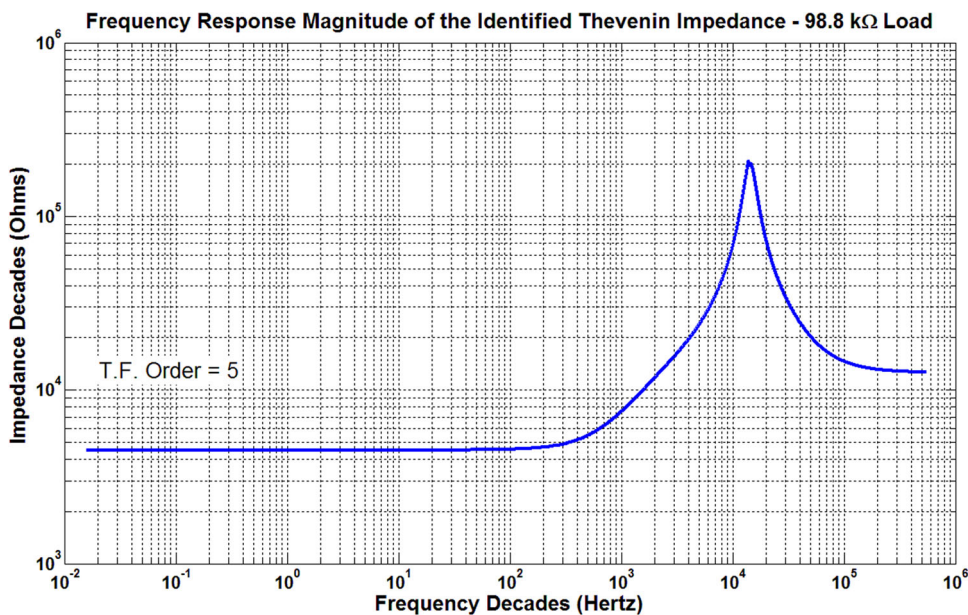


Fig. 9 Z_{th} magnitude–frequency response at log–log scale



lumped-parameter physics of the system, then Z_L should predict the known resistive output loads at the DC level. Further, the RRSE of the predicted output versus the measured output under R_{actual} should be small. Due to unmodeled measurement parasitic effect, we did not expect an ideal flat-band frequency response for the resistor-connected output. During simulation, a first-order system produced the best result for each case. The 216.6 K Ω simulated case versus the actual time response output presented in Fig. 10 represents the observed accuracy of the identification scheme. Figure 11 displays the uncertainties

mentioned for the above case that account for the finite poles and zeros. Table 2 summarizes the results of actual load, identified load, RRSE (predicted vs. measured output voltage waveform) and measurement error in DC resistance. The values give acceptable accuracy within range but suggest some variability in repeatability.

4.3 Identification of fingertip skin bio-impedance

We relied on the Cole–Cole first-order bio-impedance model Z_{bio} presented in subsection B of Sect. 2 (refer to

Fig. 10 Output-scaled time response. The graph shows the recreation of the actual output measured against a 216.6 kΩ standard by simulating the identified Z_L

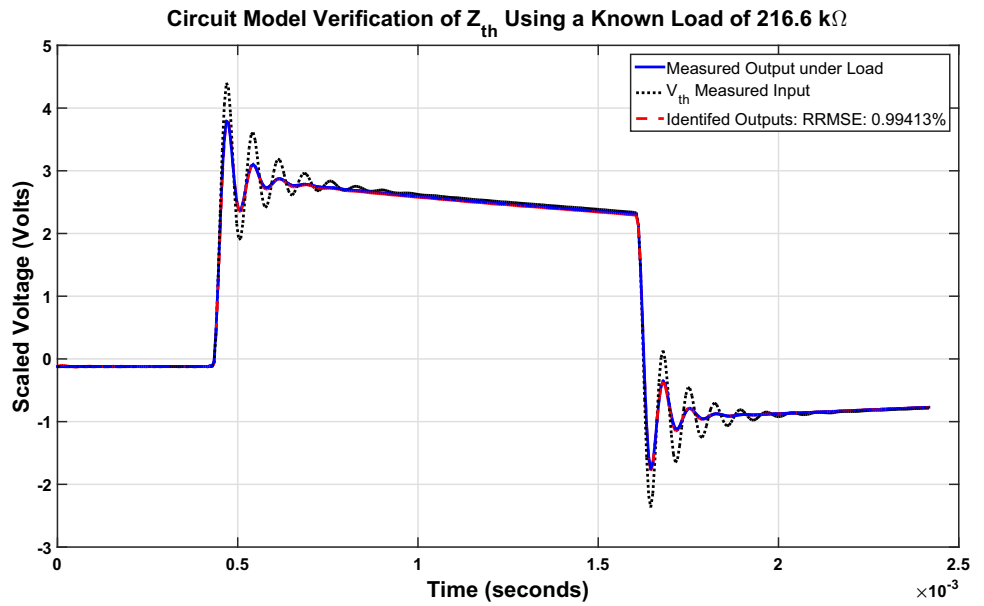


Fig. 11 Output-scaled frequency response. The graph shows the re-creation of the actual output measured against a 216.6 kΩ standard by simulating the identified Z_L

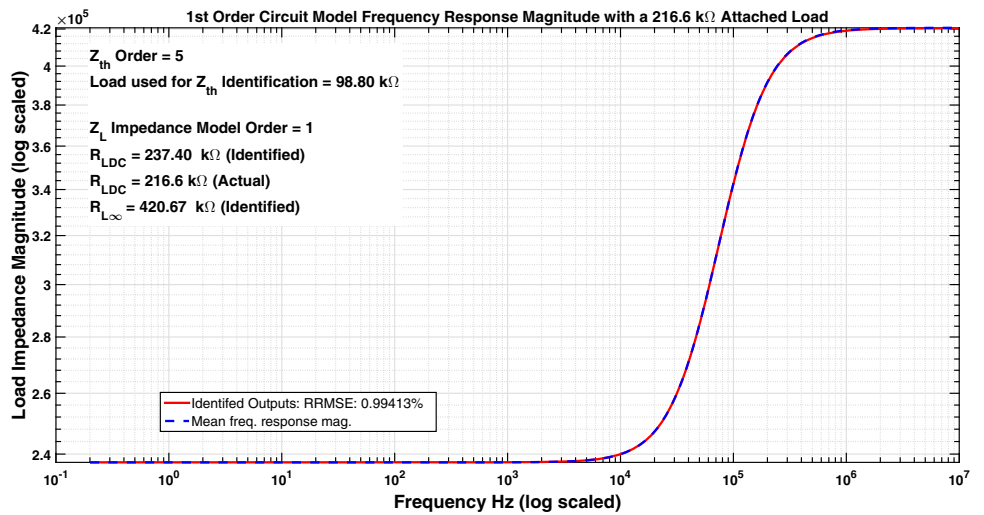


Table 2 Reliability tests of identification algorithm

Actual R (kΩ)	Identified R (kΩ)	RRSE	Error % of actual vs. identified (%)
21.62	20.70	13.45	4.26
55.20	55.43	4.31	0.42
216.6	237.4	0.99	9.60
328.9	368.9	8.65	12.2
555.0	556.4	4.31	0.25

Fig. 3). The human load impedance model in the s -domain is:

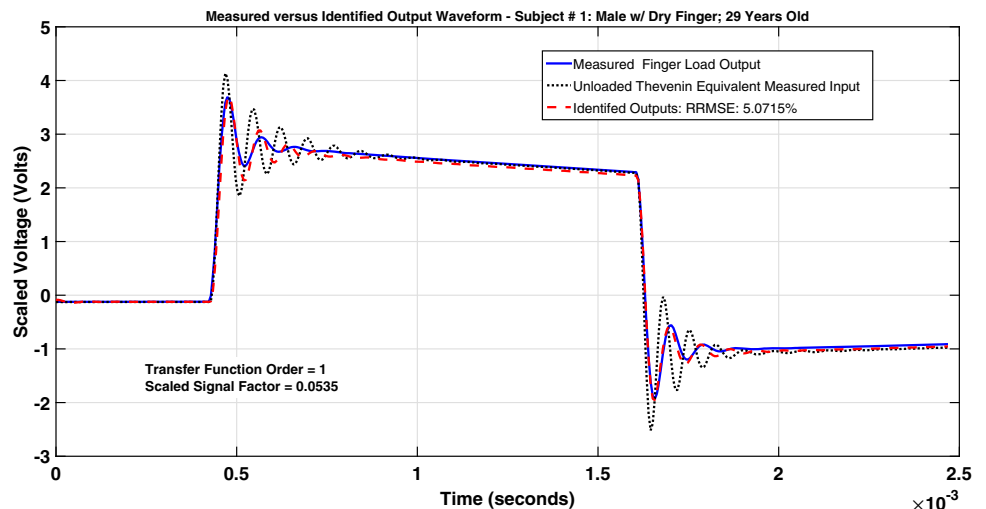
$$Z_{\text{bio}}(s) = \frac{(R_s + R_p) + R_s R_p C_p s}{1 + R_p C_p s} \tag{8}$$

From the driver and load model circuit, we derive the following relation:

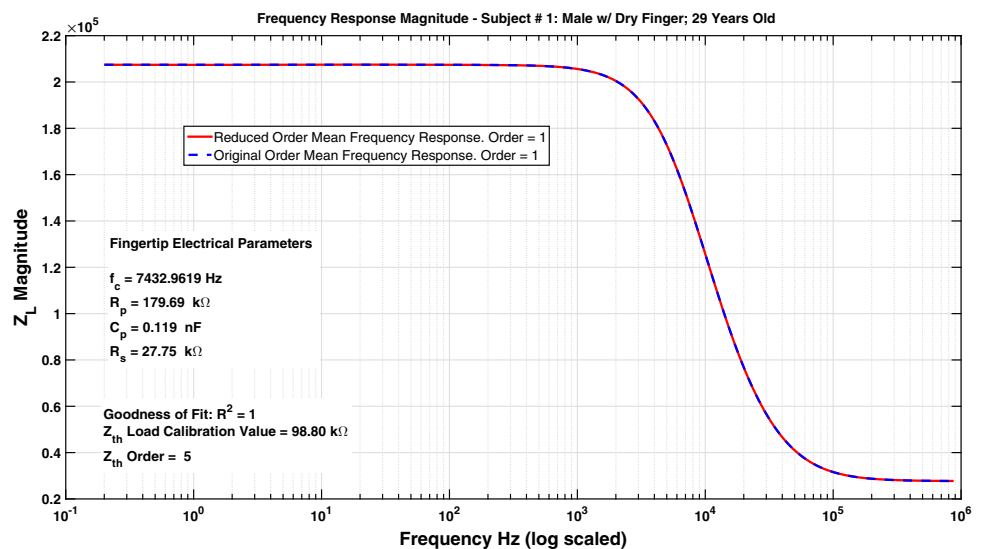
$$D_{\text{bio}_i}[Z_{\text{th}}V_{\text{out}}] = N_{\text{bio}_i}[V_{\text{th}} - V_{\text{out}}], \tag{9}$$

where Z_{th} is the identified driver circuit impedance described in Eq. (5), and N_{bio_i} and D_{bio_i} constitute the numerator and denominator of Z_{bio} , respectively. The reformulated input and output vectors in Eq. (1) are now:

Fig. 12 a One of 20 voltage outputs (typical) under dry index fingertip load; **b** frequency response and identification parameters based on **a**



(a)



(b)

$$X = V_{th} - V_{out} \quad \text{and} \quad W = Z_{th}V_{out}. \tag{10}$$

Then, using the asymptotic value $Z_{bio_{\infty}}$ and Eq. (8), the program derives the physical parameters of the user’s RC-modeled bio-impedance:

$$Z_{bio_{\infty}} \left(\frac{1}{C_p R_p} = s_c \right) = \frac{(2R_s + R_p)}{\sqrt{2}} \tag{11}$$

$$R_s = Z_{bio_{\infty}}(\infty) \tag{12}$$

$$R_p = Z_{bio_{\infty}}(0) - R_s \tag{13}$$

We produced 20 RC models based on Eq. (8) under a dry index fingertip load for one subject to test the method’s repeatability. An additional 12 models were produced under dampened fingertip measurements. For the

dampened index case, the subject placed his finger in untreated tap water and briefly rubbed it into the skin. This process is an attempt to mimic the ion solute found in sweat production. Figure 12a and b show one of 20 results under a dry index and, similarly, Fig. 13 (a) and (b) for the damp fingertip case. Corresponding to the above experiments on both dry and damp fingertip, Tables 3 and 4 give the mean \bar{X} and standard deviation s of each of the calculated values in Eqs. (11 ~ 13) along with the calculated low-pass corner frequency f_c and RRSE. The largest variability in percentage occurs with R_s . This may be a consequence of its reduced influence on the amplitude of the loaded square wave output transients and $R_p \gg R_s$ in Eq. (8). As such, the small $R_s C_p$ product locates the zero of the load network at a much higher frequency than the bio-impedance pole

Fig. 13 a One of 12 voltage outputs (typical) under damp index fingertip load; **b** frequency response and identification parameters based on **a**

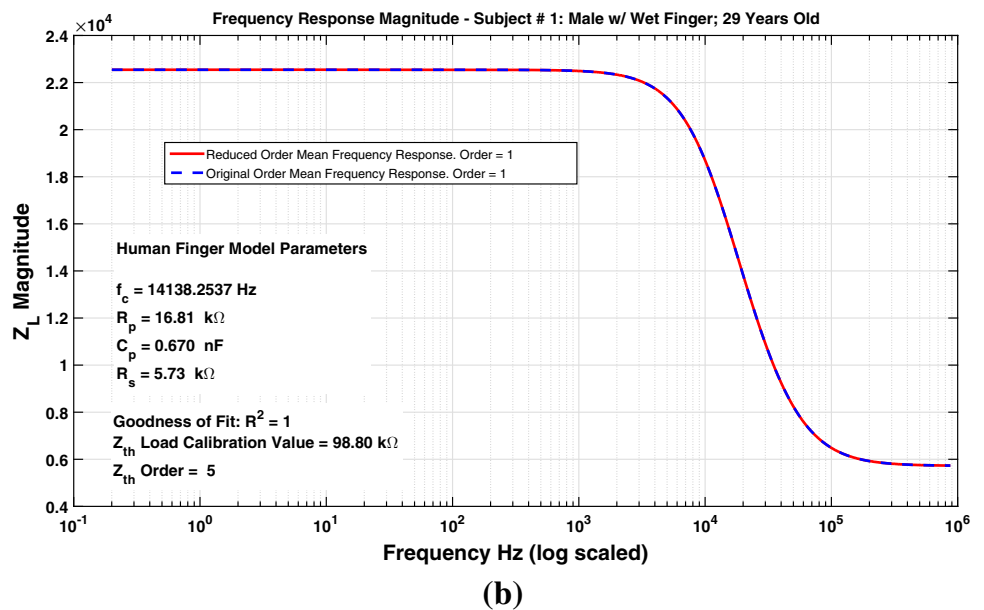
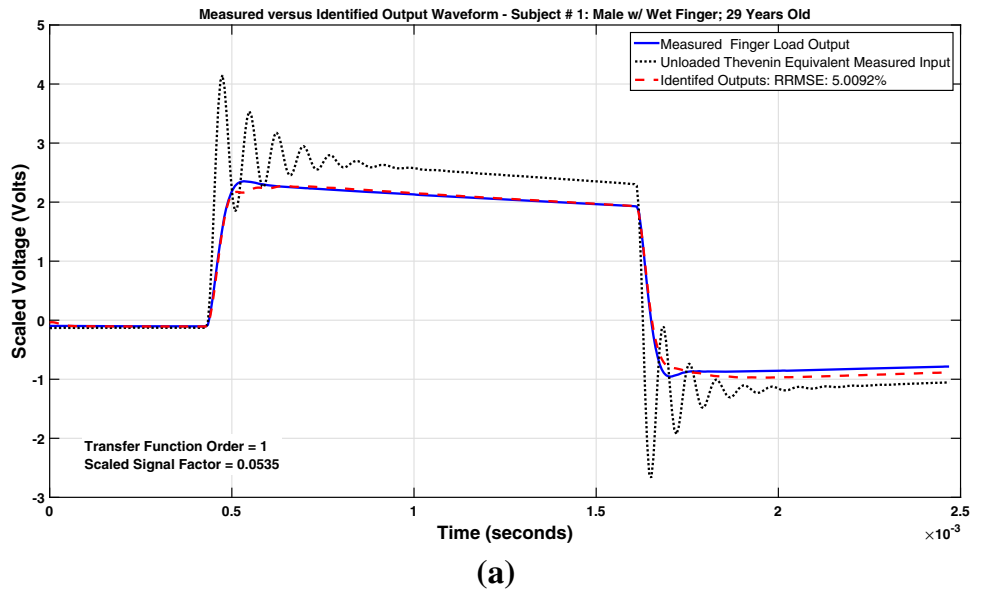


Table 3 Summary statistics (ref. Fig. 3) ($n = 16$ I/O combinations): one subject dry index fingertip—male, 29 years old

Stat	f_c (kHz)	R_p (k Ω)	C_p (nF)	R_s (k Ω)	RRSE (%)
\bar{X}	8.33	185.96	0.12	33.40	6.38
s	3.34	55.32	0.04	15.24	1.53

Table 4 Summary statistics (ref. Fig. 3) ($n = 12$ I/O combinations): one subject damp index fingertip—male, 29 years old

Stat	f_c (kHz)	R_p (k Ω)	C_p (nF)	R_s (k Ω)	RRSE (%)
\bar{X}	14.79	17.36	0.66	6.14	4.97
s	4.35	3.35	0.10	1.43	1.37

Table 5 Circuit element values for modeling the identified dry finger bio-impedance

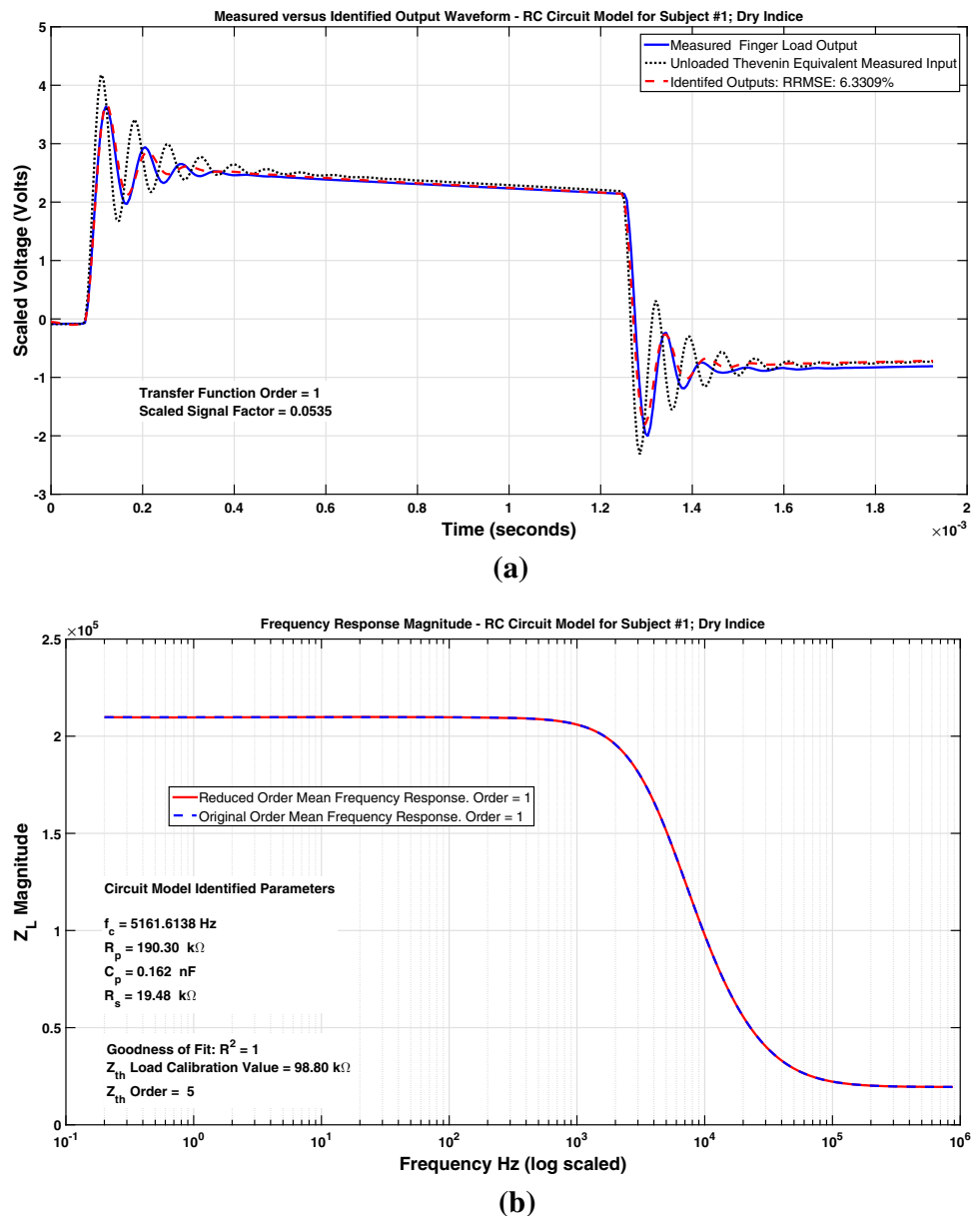
Element	R_p (k Ω)	C_p (nF)	R_s (k Ω)
–	179.8	0.12	32.46

Table 6 Summary statistics (ref. Fig. 3) ($n = 23$ I/O combinations): actual versus identified circuit elements

Element	R_p (k Ω)	C_p (nF)	R_s (k Ω)	RRSE (%)
Actual	179.8	0.120	32.46	***
\bar{X}	184.34	0.134	27.43	6.39
s	32.32	0.036	11.85	2.03
% Error	2.46 %	10.40 %	15.50 %	***

***means no value or it is not appropriate for any value

Fig. 14 **a** One of 23 voltage outputs (typical) under the constructed RC circuit load; **b** frequency response and identification parameters based on **a**



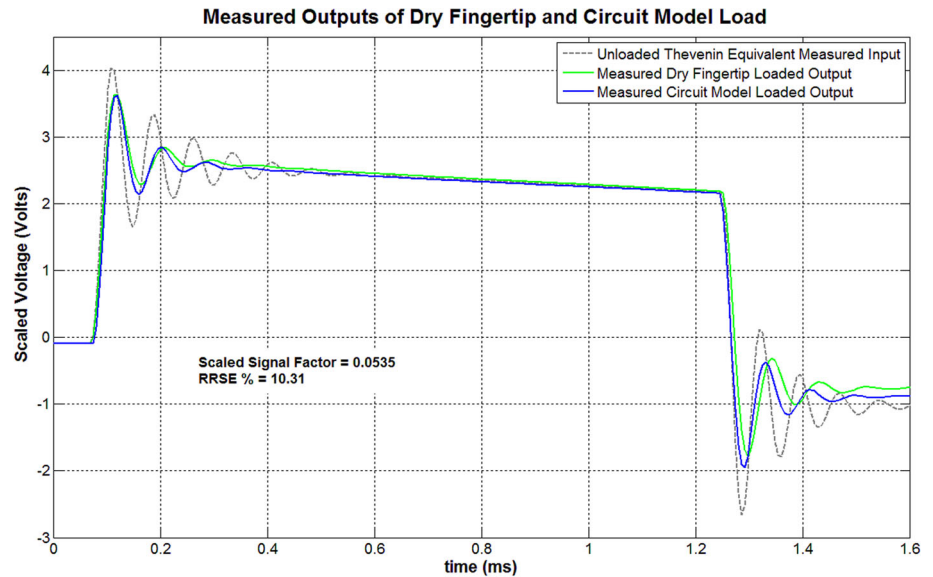
location; hence, the bandwidth limitations resulting from the finite Nyquist sampling rate coupled with measurement noise, amplifier slew rate, and high-frequency parasitic elements from the measurement probes and wires all strongly influence the zero location of the network and thus manifest in the resulting R_s sensitivity. Conversely, R_p mainly determines the pole location and subtly influences the zero due to its larger magnitude. This value then heavily determines the shape of the loaded output and should vary the least, as is seen. C_p strongly influences both the pole and zero location and shows a variability intermediate of R_p and R_s as expected (Table 5).

In addition, we built a representative RC model of the identified electrical characteristics of our subject’s dry fingertip to test the accuracy of the identification and

validity of the proposed model illustrated in Fig. 3 using the following procedures: 1) comparing the element-wise closeness of fit of the identified RC load and the actual values; and 2) investigating the subject’s dry fingertip identification and measurement output versus that of this circuit, respectively. The parameters shown in Table 6 highlight the values chosen to build the circuit model for this experiment and reflect the mean identified parameters in Table 6 within 5% tolerance each. The outputs were measured under the same input conditions presented in Table 1.

A total of 23 RC models were also produced from Eq. (8) by combining multiple input/output measurement trials, without encountering any outliers. Figure 14a and b display the model’s RC circuit output and frequency

Fig. 15 Figure plots of Thévenin voltage along with measured dry fingertip and associated model loaded output; scaled by 0.0535; RRSE = 10.31% between loaded outputs



response used for one system identification trial, respectively. Figure 15 graphs the display terminal outputs under dry fingertip load and the RC modeled circuit. Table 6 summarizes the statistical results for the RC model's loaded outputs for all 23 trials. The means \bar{X} of the identified circuit elements for all these identification trials agree with the magnitudes of the actual circuit elements, which suggests an accurate identification method. Also, the small standard deviation s for each resistive or capacitive element suggests that the identification scheme achieves high repeatability with each test result. As discussed, this is consistent with the dry fingertip bio-impedance identification tests, in that R_p varies the least, C_p exhibits intermediate variability, and R_s varies the most, as shown in Table 6. Finally, as observed in both Tables 3 and 6, the mean tendency of the RC model and bio-impedance system identification result in similar parameter values. From this, we conclude that the results of this test subject's bio-impedance signature validates the selected Cole–Cole model for the specified operating conditions and stimulating waveform shape and configuration.

5 Conclusions and future work

In this paper, a fingertip skin bio-impedance identification algorithm for the enhancement of electro-tactile rendering is investigated for two skin moisture regimes. The algorithm assumes a first-order RC impedance network for identification purposes. We show validity of the identified parameters of the subject by building a model and quantitatively comparing the voltage output from the model with the voltage output from the fingertip skin identified

parameters for our specified operating conditions. We also demonstrate the reliability of the identification scheme by comparing the deviations among multiple trial runs of both the human and known model identifications.

Future work will involve incorporating a feedback control scheme for adjusting the input in real time based on the measurements. The next step then hinges on integrating the sampling and identification hardware and software with the electro-tactile-based rendering device in a compact

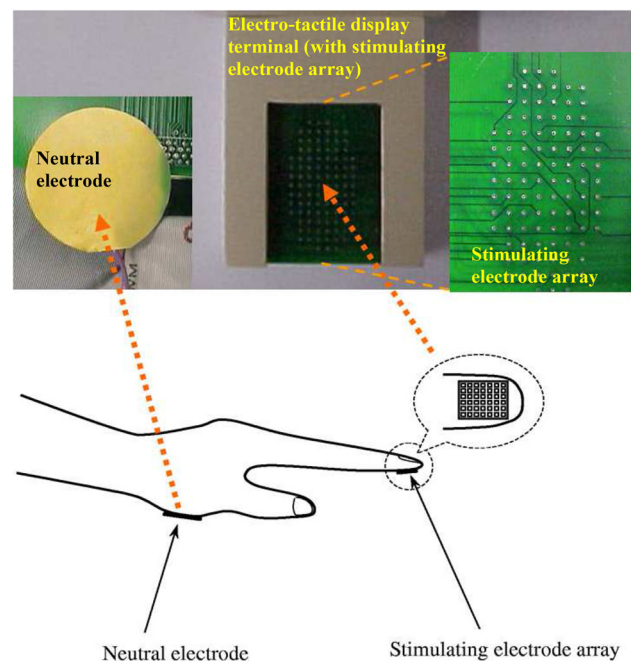


Fig. 16 Electro-tactile display terminal and electrode placement: large neutral electrode is placed on palm thenar, index fingertip touches the stimulating electrode array

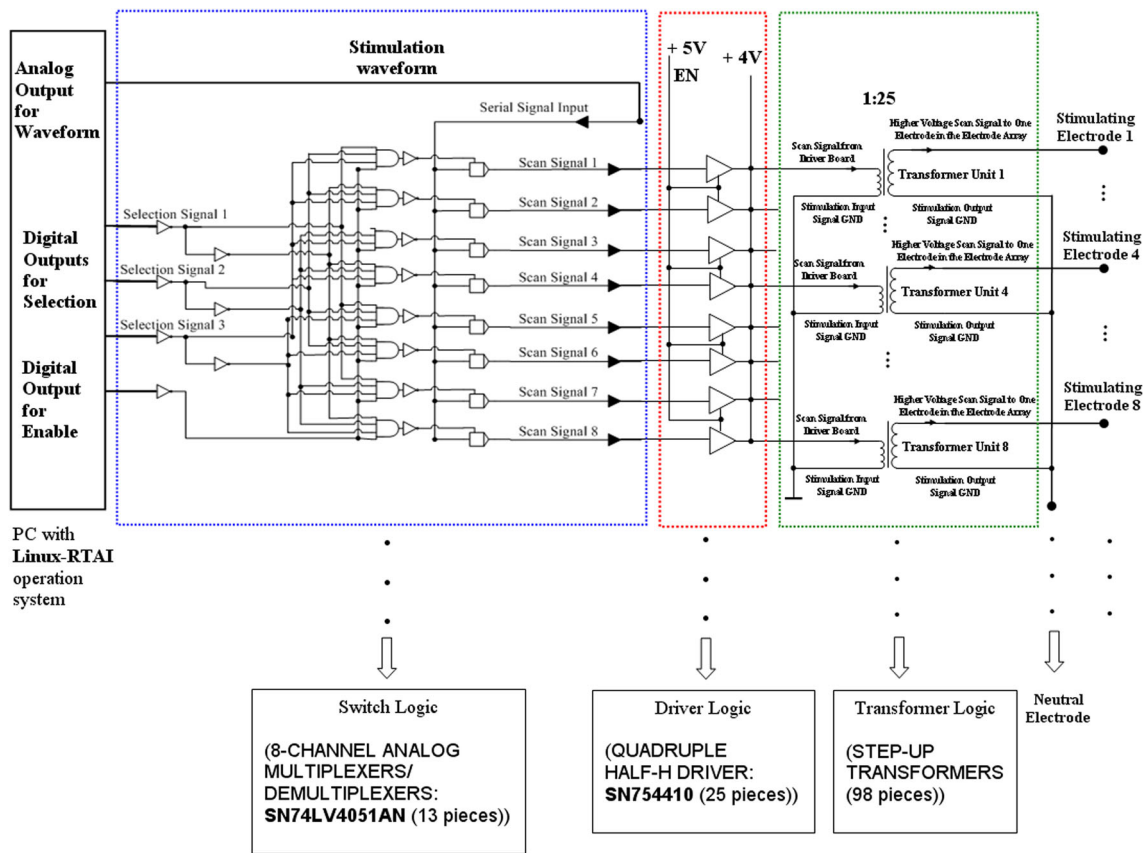


Fig. 17 Logic diagram of the driver circuitry of electro-tactile display system

module. Ideally, the user need only place his or her fingertip on the display terminal, and the identification program is initiated by monitoring the differential loading condition. The resulting calculation of the user’s bio-impedance signature then tailors, to a comfortable level, the current amplitude of the stimulating waveform in a short period of time.

Acknowledgements This work was supported in part by National Science Foundation (NSF) CAREER Award CBET-1352006 and National Institutes of Health (NIH) grant R01EY026275.

Appendix: The custom-built electro-tactile display

Electrode array of electro-tactile display

The developed electro-tactile display is an electrode array device that evokes tactile (touch) sensations within the fingertip skin by passing a local electric current through the skin to stimulate afferent nerve fibers or receptors via the electrodes placed on the skin surface. To ensure safety, a protective circuit is included in the display.

Electro-tactile stimulation needs both stimulating electrodes and a neutral electrode return. In our design, the small

electrode array is used as the stimulating electrode array, and is shown in Fig. 16. As shown, the array for the fingertip (index) has 98 stimulation electrodes within an area measured $25 \times 12 \text{ mm}^2$. Each electrode area is 0.454 mm^2 with a density of 32 electrodes per cm^2 and spaced 2 mm apart from one another. These values are roughly consistent with reported spatial resolution of the relevant tactile receptors at the fingertips (Bobich et al. 2007; Kajimoto et al. 2004; Shen et al. 2006; Kaczmarek and Webster 1991). The electrode array board is a custom-manufactured printed circuit board (PCB). The designed fingertip-shaped cross section of the display terminal helps to conform the index fingertip. Another large electrode (706.5 mm^2) is used as the neutral electrode and is located in the thenar area close to the thumb. According to the arrangement of the electrodes, the stimulating current will pass through the fingertip skin at multiple locations of the electrode array and then move to the neutral electrode (like ground) through the tissues between the fingertip and the thenar. Figure 16 also shows the placement of two electrode pieces in the developed electro-tactile display terminal.

In addition, considering the electrochemistry between electrodes and the skin of the human finger ((Kaczmarek and Tyler 2000; Poletto and Doren 1999; Kaczmarek and

Webster 1991; Neuman 1998; Rattay 1990), conductive copper is used for the material of both the neutral and stimulating electrodes.

Driver circuitry of electro-tactile display

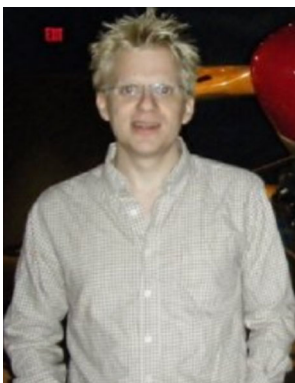
The logic diagram of the developed electro-tactile driver circuit is shown in Fig. 17. As the diagram shows, the circuit includes three basic units: PC-controlled switch logic unit for generating the scanning signals to the array, the driver unit for driving the scanning signals to the step-up transformer unit, and the step-up signals from the transformer outputs to the electrode array for stimulation.

Figure 17 also shows the electro-tactile display circuit for concurrent row scanning of eight-channel signals onto the respective electrodes of the display terminal. There are a total of 13 of these structures, allowing for 104 addressable electrodes (we used a 98-electrode array). The analog output channel from the computer acts as input to the current drivers. Each current driver delivers its output to its respective input of one of the 1:25 step-up transformers. Three digital selection lines and one of the 13 select lines address the analog demultiplexer to pass the analog signal to the “on” current drivers for a particular eight-bit row scan. The current drivers can feature voltage output amplitude level programmability, allowing for variable stimulation amplitudes displayed on the electrodes. To improve the scanning speed, real-time implementation of the electro-tactile stimulation was performed using an x86-based PC running a Linux operating system. The RTAI (RealTime Application Interface) patch was used to provide POSIX-compliant, real-time functionality to the Linux OS (see [28]). The maximum output rate of the current system can be around 80KHz.

References

- Asamura, N., Yokoyama, N., Shinoda, H.: A method of selective stimulation to epidermal skin receptors for realistic touch feedback. In: Proceedings of the 1999 IEEE Virtual Reality Conference, pp. 274–281 (1999)
- Bach-y-Rita, P., Kaczmarek, K.A., Meier, K.: The tongue as a man-machine interface: a wireless communication system. In: Proceedings of the 1998 International Symposium on Information Theory and its Applications, pp. 79–81 (1998a)
- Bach-y-Rita, P., Kaczmarek, K.A., Tyler, M.E., et al.: Form perception with a 49-point electrotactile stimulus array on the tongue: a technical note. *J. Rehabil. Res. Dev.* **35**, 427–430 (1998b)
- Benali-Khoudja, K.M., et al.: Tactile interfaces: a state-of-the-art survey. In: Proceedings of the 35th International Symposium on Robotics, March 23–26 (2004)
- Bobich, L.R., Warren, J.P., Sweeney, J.D., et al.: Spatial localization of electro-tactile stimuli on the fingertip in humans. *Somatosens. Mot. Res.* **24**(4), 179–188 (2007)
- Boxtel, A.: Skin resistance during square-wave electrical pulses of 1 to 10 mA. *Med. Biol. Eng. Comput.* **15**, 679–687 (1977)
- Brannon, H., MD: Stratum Corneum—Top Layer of the Epidermis—Structure and Function. http://dermatology.about.com/od/anatomy/ss/sc_anatomy.htm. Accessed 12 Feb 2009
- De Rossi, D., et al.: Polymer based interfaces as bioinspired smart skins. *Adv. Colloid Interface Sci.* **116**, 165–178 (2005)
- Dorgan, S.J.: A model for human skin impedance during surface functional neuromuscular stimulation. *IEEE Trans. Rehabil. Eng.* **7**(3) (1999)
- Faes, T., van der Meij, H., et al.: The electric resistivity of human tissues (100 Hz–10 MHz): a meta-analysis of review studies. *Physiol. Meas.* **20**, R1–R10 (1999)
- Foster, K.R., Lukaski, H.C.: Whole-body impedance-what does it measure? *Am. J. Clin. Nutr.* **64**, 388S–396S (1996)
- Gemperle, F., et al.: Design of a wearable tactile display. In: Proceedings of the 2001 Fifth International Symposium on Wearable Computers, pp. 5–12 (2001)
- Haase, S.J., Kaczmarek, K.A.: Electrotactile perception of scatterplots on the fingertips and abdomen. *Med. Biol. Eng. Comput.* **43**, 283–289 (2005)
- Kaczmarek, K.A., Tyler, M.E., Rita, P.B.: Electro-tactile haptic display on the fingertips: preliminary results. In: Proceedings of the 16th IEEE International Conference on Engineering on Medicine and Biology, pp. 940–941 (1994)
- Kaczmarek, K.A., Tyler, M.E.: Effect of electrode geometry and intensity control method on comfort of electro-tactile stimulation on the tongue. In: Proceedings of the ASME Dynamic Systems and Control Division (2000)
- Kaczmarek, K.A., Webster, J.G.: Voltage-current characteristics of the electrotactile skin-electrode interface. In: Proceedings of the Annual International Conference of the IEEE Engineering in Medicine and Biology Society, vol. 11, pp. 1526–1527 (1989)
- Kaczmarek, K.A., Webster, J.G., et al.: Electrotactile and vibrotactile displays for sensory substitution systems. *IEEE Trans. Biomed. Eng.* **38**(1), 1–15 (1991)
- Kajimoto, H., et al.: Tactile feeling display using functional electrical stimulation. In: Proceedings of the 9th International Conference on Artificial Reality and Telexistence. Virtual Reality Society of Japan, pp. 107–114 (1999)
- Kajimoto, H., Kawakami, N., Maeda, T., et al.: Electrocutaneous display with receptor selective stimulations. *Electron. Commun. Jpn. Part 2* **85**(6), 40–49 (2002)
- Kajimoto, H., Kawakami, N., Tachi, S., et al.: SmartTouch: electric skin to touch the untouchable. *IEEE Comput. Graph. Appl. Emerg. Technol.* **24**(1), 36–43 (2004)
- Koo, I., et al.: Wearable Fingertip tactile display. *SICE-ICASE International Joint Conference*, pp. 1911–1916 (2006)
- Ljung, L., Soderstrom, T.: Theory and Practice of Recursive Identification, pp. 13–24. The MIT Press, Cambridge (1983)
- Neuman, M.R.: Biopotential electrodes. In: Webster, J.G. (ed.) *Medical Instrumentation, Application and Design*, pp. 183–232. Wiley, New York (1998)
- Phillips, J.R., Johnson, K.O.: Neural mechanisms of scanned and stationary touch. *J. Acoust. Soc. Am.* **77**(1), 220–224 (1985)
- “Pulse Transformers”, Online document. <http://www.rhombus-ind.com/app-note/circuit>. Accessed 14 Feb 2009
- Pliquett, U., Langer, R., Weaver, J.C.: Changes in the passive electrical properties of human stratum corneum due to electroporation. *Biochimica et Biophysica Acta* **1239**, 111–121 (1995)
- Poletto, C.J., Van Doren, C.L.: A high voltage, constant current stimulator for electrocutaneous stimulation through small electrodes. *IEEE Trans. Biomed. Eng.* **46**(8), 929–936 (1999)
- Prokhorov, E.F., et al.: In vivo electrical characteristics of human skin, including at biological active points. *Med. Biol. Eng. Comput.* **38**, 507–511 (2000)

- Rattay, F.: *Electrical Nerve Stimulation*. Springer, Berlin (1990)
- “RTAI”, RTAI Official Website, Dec. 10 (2008). <https://www.rtai.org/>. Accessed 1 March 2009
- Reilly, J.P.: *Electrical Stimulation and Electropathology*. Cambridge University Press, Cambridge (1992)
- Rosell, J., Colominas, J., et al.: Skin impedance from 1 Hz to 1 Mhz. *IEEE Trans. Biomed. Eng.* **35**(8), 649–651 (1988)
- Shen, Y., Pomeory, C.A., Xi, N., et al.: Quantification and verification of automobile interior textures by a high performance tactile-haptic interface. In: *Proceedings of the 2006 IEEE/RSJ International Conference on Intelligent Robots and Systems*, pp. 3773–3778 (2006)
- Shen, Y., et al.: Supermedia interface for internet based telediagnosics of breast pathology. *Int. J. Robot. Res.* **26**(11–12), 1235–1250 (2007)
- Shimojo, M., et al. (2003) Development of a system for experiencing tactile sensation from a robot hand by electrically stimulating sensory nerve fiber. In: *Proceedings of the 2003 IEEE International Conference on Robotics and Automation*, vol. 1, pp. 1264–1270
- Steiglitz, K., McBride, L.E.: A technique for the identification of linear systems. *IEEE Trans. Autom. Control* **10**(4), 461–464 (1965)
- Szeto, A.Y.J., Riso, R.R.: Sensory feedback using electrical stimulation of the tactile sense. In: Smith, R.V., Leslie Jr., J.H. (eds.) *Rehabilitation Engineering*, pp. 29–78. CRC Press, Boca Raton (1990)
- Szeto, A.Y.J., Saunders, F.A.: Electrocutaneous stimulation for sensory communication in rehabilitation engineering. *IEEE Trans. Biomed. Eng.* **29**, 300–308 (1982)
- Vallbo, A.B.: Sensations evoked from the glabrous skin of the human hand by electrical stimulation of unitary mechanosensitive afferents. *Brain Res.* **215**, 359–363 (1981)
- Vallbo, A.B., Johansson, R.S.: Properties of cutaneous mechanoreceptors in the human hand related to touch sensation. *Hum. Neurobiol.* **3**, 3–14 (1984)
- Yarimaga, O., Lee, J., Lee, B., et al.: Tactile Sensation Display with Electro-tactile Interface. ICCAS 2005, KINTEX, Gyeonggi-Do, Korea, June 2–5 (2005)
- Yarimaga, O., Lee, B., Ryu, J., et al.: An electro-tactile device for broadcasting and game applications. *HCI2005 Korea* **1**, 388–394 (2005)
- Yoon, M., Yu, K.: Psychophysical experiment of vibrotactile pattern perception by human fingertip. *IEEE Trans. Neural Syst. Rehabil. Eng.* **16**(2), 171–177 (2008)

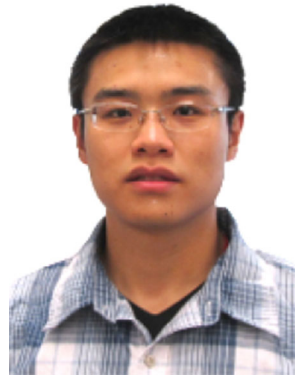


John Gregory received his master's degree from Michigan State University and is currently with the Coritech Services and TM3 Systems, Michigan, USA. His research interests lie in the areas of electro-tactile haptic systems, intelligent algorithms and applications, and sensors and actuators.



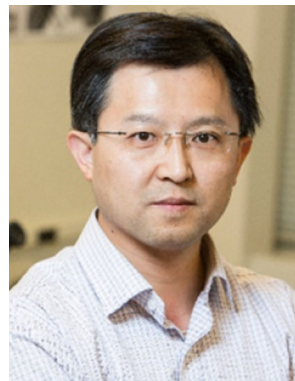
Shengchun Tang received her B.S. and M.S. degrees in mechatronics engineering from Beijing Institute of Technology, China, in 1994 and 2005, respectively. In 2005, she joined the School of Electrical Engineering, Beijing Information Science and Technology University, Beijing, China, and is currently working toward her Ph.D. degree in the School of Automation at the University of Science and Technology Beijing, China. Her research inter-

ests include controls, system identification, sensor-based robotics and applications.



Yudong Luo received a B.S. degree in electrical engineering and an M.S. degree in biomedical engineering from the University of Nevada, Reno, in 2011 and 2013, respectively, where he is currently pursuing his Ph.D. in biomedical engineering. Since 2011, he has been a research assistant with the Bioinstrumentation and Automation Lab in the Electrical and Biomedical Department, University of Nevada, Reno. He is the author of more than ten

articles. His research interests include micro/nano-force sensors, BCI systems, and bio-inspired and biomimetic robotics. Yudong Luo's awards and honors include Best Paper Award finalist at IEEE ROBIO 2014 and 2015.



Yantao Shen received his B.S. and M.S. degrees from Beijing Institute of Technology and his Ph.D. degree from the Chinese University of Hong Kong, and he is currently an associate professor in the Department of Electrical and Biomedical Engineering at the University of Nevada, Reno (UNR). His current research interests include bioinstrumentation and automation, bio-mechatronics/robotics, sensors and actuators, and tactile and haptic interfaces. Dr.

Shen has authored/coauthored one book chapter and over 100 peer-reviewed journal and conference papers, and co-holds four US patents. He was also a Best Vision Paper Award finalist in the 2001 IEEE ICRA, a Best Conference Paper Award finalist in the 2007 IEEE RO-MAN, a winner of the T.J. Tarn Best Paper Award in the 2009 IEEE ROBIO, and a Best Conference Paper Award finalist in the 2014 IEEE ROBIO. Dr. Shen is the recipient of an NSF CAREER Award and the 2015 Excellence Award in research from UNR College of Engineering, and was named UNR IEEE Outstanding Electrical Engineering Professor in both 2010 and 2011.